# Sensitive Detection of the Human Epididymis Protein-4 (HE4) Ovarian Cancer Biomarker through a Sandwich-Type Immunoassay Method with Laser-Induced Breakdown Spectroscopy

Robinson Karunanithy, Suthakaran Ratnasingam, Torrey Holland, and Poopalasingam Sivakumar*
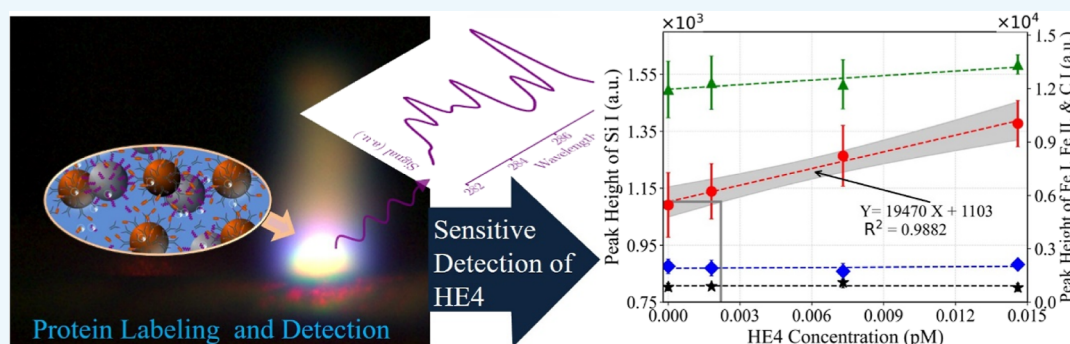
Cite This: https://doi.org/10.1021/acs.bioconjchem.2c00551

Read Online

ACCESS | Metrics & More | Article Recommendations | SI Supporting Information

**ABSTRACT:** Detection of cancer before the appearance of any symptoms is crucial for successful treatment. Early detection is, however, very challenging, particularly for the types of cancer with few or no symptoms at early stages, such as epithelial ovarian cancer (EOC). Developing a user-friendly method that can detect biomarkers with sufficient selectivity, sensitivity, and reproducibility is a promising approach for overcoming the challenges of early detection of EOC. In this study, we report a sandwich-type microparticle immunoassay for sensitive detection of the HE4 biomarker with laser-induced breakdown spectroscopy. Here, we cross-linked elemental particles to a specific functional group of the targeted biomolecules based on a covalent and non-covalent linking chemistry to improve the sensitivity and selectivity of biomarker detection, in which $Fe_3O_4$ and $SiO_2$ microparticles were used to conjugate and purify the antibody–antigen in complex media. Simultaneous detection of Fe and Si from a magnetically purified assay significantly improves the HE4 biomarker's detectability, in which HE4 was detected with a limit of detection of 0.0022 pM. We also determined the coupling ratio between HE4 and silica particles using a silicon calibration curve.

## INTRODUCTION

Epithelial ovarian cancer (EOC) is the deadliest gynecologic cancer. It has few or no early-stage symptoms and no effective screening tools. The treatment and survival solely depend on the cancer stage at diagnosis.[1−4] Over 60% of patients are diagnosed at an advanced stage and have a ~29% survival rate. In contrast, the survival rate of the localized (early) stage is ~94%; however, only 15% are diagnosed at an early stage.[1,2] According to the American Cancer Society (ACS), 19,880 women will have new diagnoses of ovarian cancer (OC), and 12,810 will die in 2022.[1] Various techniques, including transvaginal ultrasound (TVUS), Doppler imaging, pelvic examination, and blood tests for a specific protein, that is, a cancer antigen (CA125), are considered potential OC screening tools in clinical use.[1,5] However, currently, there is no recommended screening for early detection of OC due to the lack of sensitivity and specificity.[1,6] Elevated levels of CA125, a type of serum biomarker discovered in 1981, are widely used as an indication of OC. The upper limit of CA125 is usually between 30 and 35 U/mL. If CA125 is above the

marginal level, that could be a symptom of OC.[7] However, CA125 alone has relatively poor sensitivity and specificity for OC at early stages. It is elevated at only 50% among asymptomatic patients, compared to 75−90% among advanced-stage patients.[8] Although the elevated level of serum CA125 is associated with cancer progression, the source and functions of CA125 remain unclear. The level of CA125 is also elevated by many other factors, including benign conditions and other non-gynecologic reasons such as diverticulitis, uterine fibroids, endometriosis, benign ovarian cysts, tubo-ovarian abscesses, hyperstimulation syndrome, ectopic pregnancies, and physiological conditions (pregnancy and menstruation).[9−12]
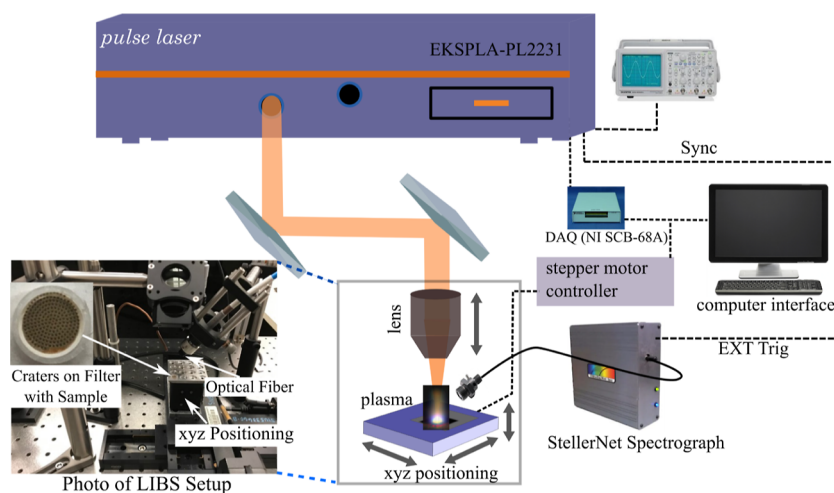
**Figure 1.** Experimental setup for LIBS and the raster pattern of the laser ablation craters on the filter with the sample (inset, magnified figure).

Various novel biomarkers such as human epididymis protein (HE4), mesothelin, and kallikreins (KLK) are being currently researched as potential standalone replacements or are being used in conjunction with CA125 for early detection of OC.[7,13−15] Remarkably, studies have shown that HE4 has higher sensitivity and specificity than all other tested biomarkers. In 2008, Havrilesky et al. studied various biomarkers, including CA125, and reported that HE4 has the highest sensitivity for early stage (I/II) and late stage (III) detection of ovarian cancer.[16] Furthermore, Moore et al. also obtained the highest sensitivity (∼72.9%) with 95% specificity when using HE4 as a single biomarker.[17] Recently, it has been approved by the Food and Drug Administration (FDA) for clinical applications.

Among the various techniques to identify proteins, immunological techniques such as the sandwich enzyme-linked immunosorbent assay (ELISA) and Western blot are some methods in practice to identify specific proteins of interest.[18−21] The immunological method is one of the most commonly used with high sensitivity and specificity, including in cancer detection.[22,23] This method is based on the natural binding ability of an antibody, also called immunoglobulin, to a specific protein called an antigen.[24−26] Although there has been some success with these methods, effective screening, early detection, and treatment remain challenging due to the lack of sensitivity, specificity, and simplicity for early cancer diagnosis in clinical trials.[27]

A slightly different approach, the sandwich-type micro-particle immunoassay method, has been successfully carried out to investigate levels of HE4 in a simulant human fluid in this study. Surface, functional group-modified particles are used to conjugate (sandwich) the antibody−antigen complex by tagging them on the particle's surface through cross-linking agents [for example, glutaraldehyde (GA)], protein A, or the avidin−biotin complex. Typically, in this method, two different types of particles are used. The first type is used to separate the antibody−antigen conjugate from other substances in the serum using magnetic separation (for example, iron micro-particles) or size filtration. The second type, typically silica or titanium, allows the detection of particles using spectroscopy techniques such as laser-induced breakdown spectroscopy (LIBS). Finally, the antigen can be quantified using the detected particle amount and a corresponding calibration curve.[27−31]

**Laser-Induced Breakdown Spectroscopy.** LIBS, a powerful analytical technique used to determine the chemical composition of materials, uses a short laser pulse to ablate a sample and form plasma. The plasma may contain excited ions, atoms, and free electrons. When the plasma cools down, the excited species emit characteristic photons as they decay into lower energy states. The emitted photons can be collected by fiber optics coupled to a spectrometer and analyzed for sample composition and content.[32,33] LIBS has been used in many fields, including the biomedical field, for quantitative and qualitative analyses due to its unique features, such as minimal or no sample preparation and being a relatively fast analysis tool. Also, it requires a tiny amount of samples for the measurements.[34,35] In quantitative analysis, calibration curves or multivariate techniques are typically utilized to get the sample's compositional information. On the other hand, reproducibility is a problem with LIBS as the spectral intensity is sensitive to laser parameters, sample distribution, and atmospheric conditions. Collecting large sets of data with multiple replications can be followed to eliminate the issues associated with reproducibility.[36−38]

Figure 1 depicts the experimental setup of the LIBS system and the raster pattern by laser ablation on a filter with the sample. A picosecond laser, EKSPLA PL2231-50-SH/TH model, equipped with an Nd: YAG/YVO4 with a 28 ps pulse duration, was used for this study. The sample on the filter was ablated using a 1064 nm wavelength and ∼19.5 mJ of energy via focusing the laser pulse on the sample surface. A motorized stage ($x−y$ directions) was used to move the sample automatically, such that there was one ablation per location. Emission light was collected using optical fiber and analyzed by a spectrometer array (StellarNet, Inc). A typical LIBS spectrum from a single pulse is shown in Figure 2.

**Data Analysis.** We collected data from three trials, each with 200 shots (pulses). After eliminating outlying data (laser ablation outside the filter, significantly lower or no LIBS signal), data sets were analyzed using the R programming language (4.1.0 version). In this regard, first, we identified a specific wavelength region that comprises the desired peak. Subsequently, we performed the baseline correction via curve fitting the background with a straight-line equation in a particular region (e.g., 287−290 nm). The peak height and area under the peak were extracted separately using the Gaussian function in the R program. Similar procedures were
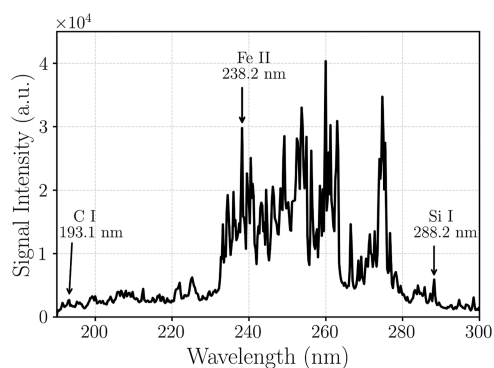
**Figure 2.** Sample LIBS spectrum corresponding to the particle ($SiO_2$ and $Fe_3O_4$)-based HE4 immunoassay system.

employed for the data obtained from each of the three trials. Two slightly different approaches (trial-to-trial and shot-to-shot) were adopted to calculate the average and standard deviations. In trial-to-trial analysis, first, we calculated the mean intensity of each trial (trials 1, 2, and 3). Then these mean values were used to compute the final mean and standard deviations. In the shot-to-shot analysis, we combined all three trials and calculated the corresponding average and standard deviation. The purpose of doing two different investigations is to determine the major contributor of signal intensity fluctuation (due to LIBS or sample preparation) by comparing each method's standard deviation. The quality of sample preparation (immunoassay system) through trial-to-trial variation and sample homogeneity and analytical method's (LIBS) reproducibility with shot-to-shot variation can be gleaned from these analyses.

## RESULTS AND DISCUSSION

**Conjugation: Variation in the Peak Height and Area with the HE4 Concentration.** Our analyses revealed that the errors (standard deviations) are relatively low from trial-to-trial compared to the shot-to-shot analysis. This appears to be due to an uneven sample distribution on the filter, which contributed to the variation in signal intensities from shot-to-shot, thus increasing the standard deviation. However, the standard deviations were comparably low for the trial-to-trial analysis as the mean values of each trial are relatively small in variation. Although Si has strong emission lines at 205.70 and 251.58 nm, Si I at 288.15 nm is selected due to minimal

influence by other emission lines, especially Fe emissions. Here, we present the results from the trial-to-trial analysis. Figure 3a,b shows the variation of the characteristic silicon peak (Si I-288.15 nm)[39−42] height (a) and peak area (b) versus the HE4 concentration. The corresponding Si I peak at 288.15 nm over the HE4 concentration is depicted in Figure 4. As one
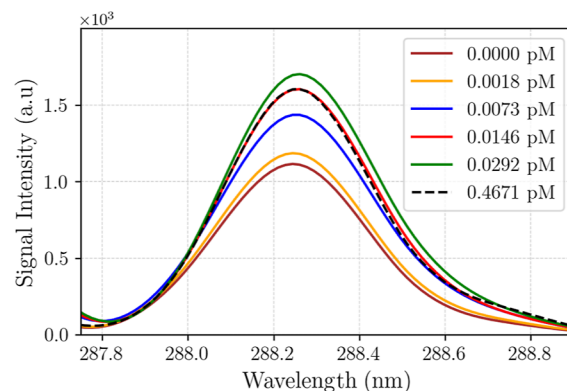


**Figure 4.** Sample spectra for Si I (baseline corrected) obtained at various HE4 concentration levels.

can see in the figures, the silicon signal count increases with the HE4 concentration in both graphs (a) and (b) of Figure 3 and in Figure 4. This is evidence that silica microparticles are conjugated on HE4. Furthermore, the intensity increased steadily at the beginning, but after a certain point, the intensity plateaued. The increasing intensity is due to a rise in bound silica particles with the increasing antigen concentration that accommodates more silica particles to bind with them.

First, to identify the working region, we performed one-way ANOVA for the combined grand data from all three trials. This was performed on the data of peak height and peak area found in the corresponding spectra of the relevant peaks in order to determine whether there were any statistically significant differences between the mean intensities at various HE4 concentrations. Next, we employed Tukey's test for a multiple comparison procedure to investigate which of the means are different. Our test results revealed significant differences between the first four points, 0.0, 0.0018, 0.0073, and 0.0146 pM, and their trend is linear. Similar results were obtained for both the height and area.


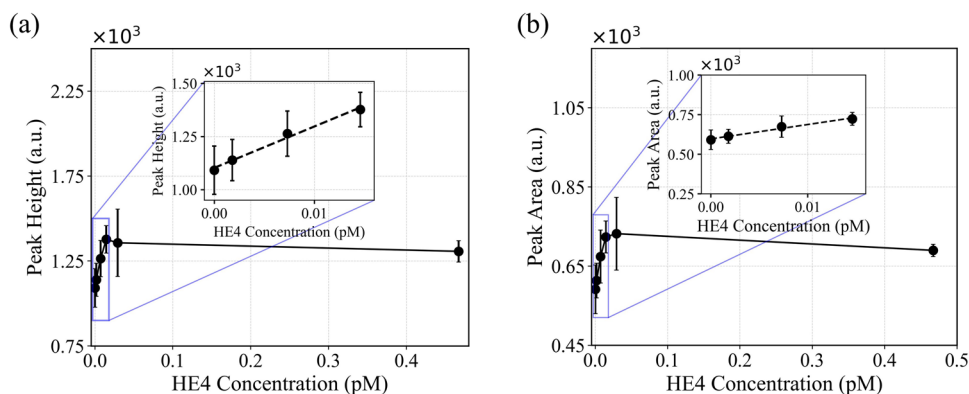
**Figure 3.** Variation in silicon (Si I) emission intensity with HE4 concentration; (a) peak height with a magnified inset graph of the linearly increasing region; and (b) peak area with a magnified inset graph of the linearly increasing region.
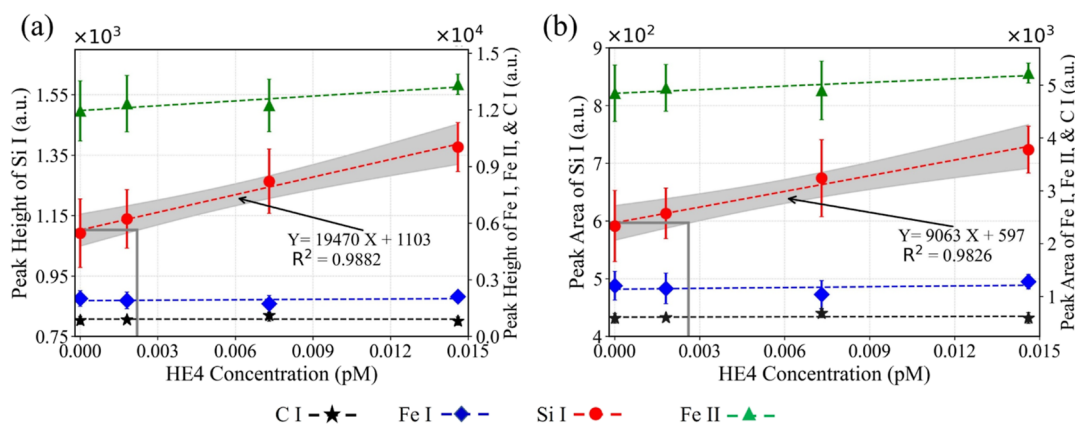
**Figure 5.** Variation in Si I, C I, Fe I, and Fe II emission lines within the working region.

However, we chose the range between 0.0 and 0.0073 pM as the working region of this assay by leaving out the point 0.0146 pM because the peak height and area corresponding to this concentration were out of our calibration curve (discussed later). After this point (from 0.0146 to 0.5 pM in Figure 3), the intensity flattened (or slightly decreased) as the HE4 concentration increased. This is due to the saturation of the HE4 antigen-binding sites. We used more silica microparticles (more than twice the amount of HE4) than the number of antigens to ensure enough silica particles could conjugate with HE4. The flattening trend suggests that from 0.0146 pM and up, all of the antibodies on the iron particles were occupied by antigens, and therefore, the maximum number of silica particles were bound with HE4 at this concentration.

Figure 5 shows the working region of the assay with three other emission lines that were used to contrast the variation in the silicon emission. We performed the same peak analyses (height and area, respectively) for the emission of iron and carbon to monitor their variation with HE4 concentrations. For this purpose, we chose two (neutral and ionized) iron emission lines, Fe I (388.76 nm)[42,43] and Fe II (238.20 nm),[39,42] which are stronger and minimally interfere with other emission lines, and a carbon (C I) emission at 193.12 nm.[39,42,44] As described in the Materials and Methodology, the amount of iron particles used in this experiment was kept at a constant amount of 50 $\mu$g. Furthermore, we used similar filters for each LIBS measurement to mitigate fluctuations in the contributing carbon emissions. Therefore, we expected iron and carbon emission lines to be relatively consistent for each concentration of HE4, as opposed to the silicon line increasing with the increasing HE4 concentrations. As shown in Figure 5, these lines did not show any particular variation as opposed to the Si I line at ~288.2 nm. Instead, the average intensities of each line were relatively similar at each concentration of HE4, only with slight fluctuations in their intensities. The fluctuations can arise from various contributions, including fluctuations in laser pulse, inconsistency in plasma position, inverse bremsstrahlung radiation and plasma, and atmospheric gas interactions.[45] The matrix effect can also play a role in signal fluctuation. A matrix effect could appear since the proportion of constituents of the conjugate, particularly the amount of silica, changes as HE4 concentration varies. Furthermore, the uneven distribution (inhomogeneity) of the particles on the filter can cause signal fluctuations on each laser shot. These factors can influence the plasma temperature and electron density, which determine the LIBS intensity.[34,46−48]

To analyze the variation of these reference emission lines with the HE4 concentration more thoroughly, we also performed one-way ANOVA for both the peak height and area data of these lines, as we had done for Si I. Table 1

**Table 1. p-values Obtained from Tukey's Multiple Comparison Test for Pairwise Comparison of Conjugation Data at 95% Family-Wise Confidence Level**

| Concentration pairs (pM) | p-values | | | | | | | |
|---|---|---|---|---|---|---|---|---|
| | For height | | | | For area | | | |
| | Si I | Fe I | Fe II | C I | Si I | Fe I | Fe II | C I |
| 0.0000−0.0018 | 0.0011 | 0.0265 | 1.0000 | 1.0000 | 0.0105 | 0.1134 | 0.0385 | 0.3990 |
| 0.0000−0.0073 | 0.0000 | 0.0000 | 1.0000 | 0.9993 | 0.0000 | 0.0000 | 0.3870 | 0.0000 |
| 0.00018−0.0073 | 0.0000 | 0.0000 | 1.0000 | 0.9991 | 0.0000 | 0.0000 | 0.9345 | 0.0000 |

summarizes the results obtained for all four emission lines. The p-values for the Tukey multiple comparison test at a 95% family-wise confidence level and the results of all pairwise comparisons are presented below. (See the Supporting Information for the complete table.)

The p-values for Si I (both height and area) indicate that there were significant differences (p-values less than 0.025) between the first three points (0.0, 0.0018, and 0.0073). In contrast, the corresponding values for the other three peaks were greater than 0.025, except for the highlighted pairs. These values suggest that for a particular emission line, there were no significant differences between the mean intensities at different concentrations of HE4. With one-way ANOVA analysis (Table 1), there can be seen considerable differences in intensities for Fe I in both the analyses of the height and area between the points 0.0, 0.0073 and 0.0018, 0.0073 and for C I (area only) between the same points as with Fe I. These differences come from the matrix effect, uneven sample distribution, fluctuations in plasma, pulse, etc., as elaborated before.

With the HE4 zero concentration (control experiment), there was a signal count to the silicon emission. However, ideally, silicon emission should be zero since there are no HE4 antigens that have the binding site for the silica particles. However, our analysis found the negative control for the peak height and area to be 1087 and 589 a.u., respectively, in the control experiment. This can be explained by the cross-coupling of silica particles with antibodies and protein A-modified iron particles. The conjugate medium contained protein A-modified iron particles and antibody-conjugated iron
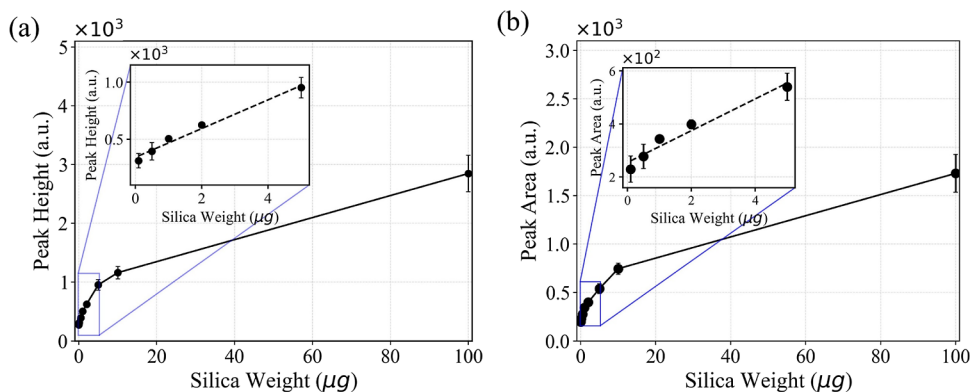
**Figure 6.** Variation in silicon intensity [(a) height and (b) area] with increasing silica.
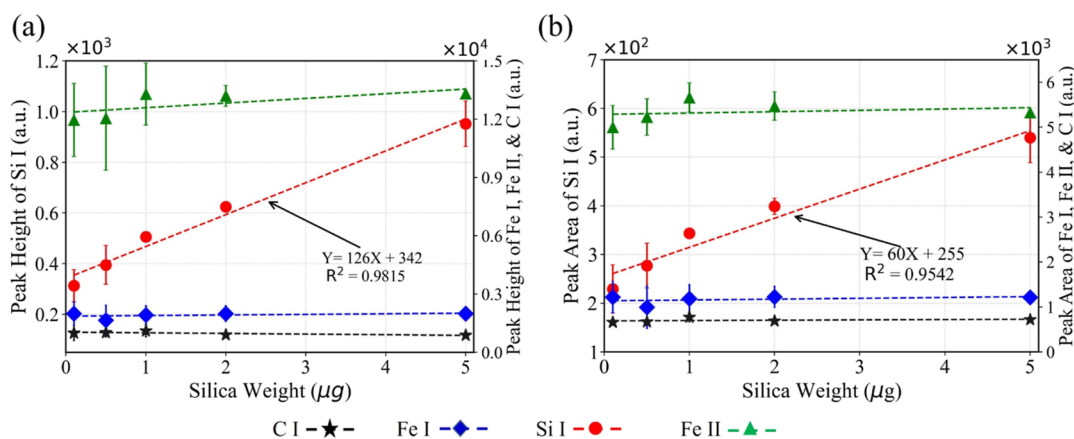


**Figure 7.** Variations in Si I, C I, Fe I, and Fe II emission lines within the best calibration region (a) showing peak height and (b) peak area.

particles, in addition to HE4-conjugated iron particles. Upon mixing GA-modified silica particles with the conjugates, they might undergo a non-specific interaction with protein A-coated iron particles and also with the antibody-coupled iron particles. These non-specified conjugates can still exist along with the specified conjugate after magnetic separation. Therefore, the silicon particles from these non-specific conjugates contributed to the signal, even though there were no HE4 antigens to bind with the silica.

To verify this further, we did another control experiment in which the protein A-coated iron particles were directly mixed with GA-modified silica particles. For this conjugate, we got a silicon peak with 1016 and 525 a.u. for the height and area, respectively. This decrease, compared to the particles with antibodies (1087 and 589 a.u.), suggests that the amount of non-specific binding decreased when there were no antibodies in the medium, suggesting that a cross-coupling of silica with the antibodies also occurs. In a control experiment, we measured the LIBS on protein A-coated iron particles with silica particles without HE4 to determine the cross-coupling of silica with the protein A-coated iron particles. The silica emissions present—646 and 375 a.u., respectively, for the peak height and area—suggest a conjugation between the silica particles and protein A-coated iron particles.

The limit of detection (LOD) of this assay was estimated (in accordance with Zaytsev et al.) at the concentration corresponding to the coincident point for the intercept and the lower boundary of the confidence band of the linear fit (solid lines indicated in Figure 5).[49] Accordingly, we found the

LOD at 0.0022 and 0.0026 pM for peak height and area analyses, respectively.

**Estimating the Amount of Bound Silica Particles and Coupling Ratio Using the Calibration Curve.** The variations in peak height and area with an increasing amount of silica particles (0.0, 0.01, 0.1, 0.5, 1, 2, 5, 10, and 100 $\mu$g) are depicted in Figure 6. As is noticed in the small graph, there was a steady increase in the intensity of silicon emission until 5 $\mu$g. After this, the rate of increase noticeably declined (5−100 $\mu$g). A linear region of the calibration curve is required to calculate the amount of bound silica particles by relating the intensity of the working region to the calibration curve. To identify the appropriate portion of the calibration graph, one-way ANOVA calculations and Tukey multiple comparison tests were performed, as had been done with the conjugation data. Based on the multiple comparison test procedure, we identified that the best calibration values lie between 0.1 and 5 $\mu$g.

Figure 7a,b shows the variation in peak height and area (respectively) of Si I emission within the linear range of calibration. To monitor Fe I, Fe II, and C I variations, relevant calculations of these emissions are also included in the same graph. As one can see in Table 2, the p-values for Si I suggest that there were differences in intensities of silicon emission at various weights. Conversely, the p-values for other lines (except the highlighted values) indicate no significant variations of the C and Fe emissions, as opposed to those of Si. The corresponding pairs of highlighted values have substantial differences due to the matrix effect, uneven sample distribution, fluctuations in plasma and laser pulse, etc.

E

**Table 2. *p*-values Obtained from Tukey's Multiple Comparison Test for Pairwise Comparison of Calibration Data at the 95% Family-Wise Confidence Interval Level**

| Silica mass pairs (µg) | p-values | | | | | | | |
|---|---|---|---|---|---|---|---|---|
| | For height | | | | For area | | | |
| | Si I | Fe I | Fe II | C I | Si I | Fe I | Fe II | C I |
| 0.1-0.5 | 0.0000 | 0.9999 | 1.0000 | 1.0000 | 0.0000 | 0.0000 | 0.0000 | 0.9690 |
| 0.1-1.0 | 0.0000 | 1.0000 | 1.0000 | 1.0000 | 0.0000 | 0.8899 | 0.0000 | 0.0000 |
| 0.1-2.0 | 0.0000 | 1.0000 | 1.0000 | 0.9999 | 0.0000 | 0.0130 | 0.0000 | 0.0159 |
| 0.1-5.0 | 0.0000 | 1.0000 | 1.0000 | 0.9999 | 0.0000 | 0.5544 | 0.0000 | 0.0000 |
| 0.5-1.0 | 0.0000 | 1.0000 | 1.0000 | 1.0000 | 0.0000 | 0.0000 | 0.0000 | 0.0000 |
| 0.5-2.0 | 0.0000 | 0.9999 | 1.0000 | 1.0000 | 0.0000 | 0.0000 | 0.0000 | 0.4536 |
| 0.5-5.0 | 0.0000 | 1.0000 | 1.0000 | 1.0000 | 0.0000 | 0.0000 | 0.0410 | 0.0000 |
| 1.0-2.0 | 0.0000 | 1.0000 | 1.0000 | 0.9999 | 0.0000 | 0.3489 | 0.0128 | 0.0000 |
| 1.0-5.0 | 0.0000 | 1.0000 | 1.0000 | 0.9999 | 0.0000 | 0.9997 | 0.0000 | 0.0000 |
| 2.0-5.0 | 0.0000 | 1.0000 | 1.0000 | 1.0000 | 0.0000 | 0.6998 | 0.0778 | 0.0043 |

Table 3 summarizes the amount of silica bound with HE4 at different concentrations within the working region and also the

**Table 3. Estimated Bound Silica Particles and the Coupling Ratio of Silica to HE4**

| HE4 concentration (pM) | predicted bound silica by 1:1 coupling (µg) | experimentally bound silica (µg) | | experimental silica to HE4 coupling ratio | |
|---|---|---|---|---|---|
| | | by peak height | by peak area | by peak height | by peak area |
| 0.0000 | 0.00 | 5.65 | 5.60 | NA | NA |
| 0.0018 | 0.23 | 0.38 | 0.37 | 1.64 | 1.64 |
| 0.0073 | 0.92 | 1.37 | 1.38 | 1.50 | 1.50 |

number of cross-coupled particles when HE4 was not present. For this purpose, we first found the Si I peak height and area at different HE4 concentration levels. Then, these values were substituted in the calibration equation to find the relevant silica weights, and then lastly, the number of bound silica particles was calculated.

## TOWARD PRACTICAL APPLICATIONS AND CHALLENGES

Implementing microparticle immunoassays in clinical trials would be beneficial for sensitive detection. The average marginal level of HE4 concentration is 70 pM. Since this technique enables one to detect low concentrations, a routine test could find even slight variations in HE4 at low concentrations, potentially predicting the potential risk of ovarian cancer at an early, treatable stage. However, the selectivity and specificity of this assay must be evaluated before applying them directly to clinical trials (see the Supporting Information for more details on selectivity and specificity). Upon the satisfactory results of selectivity and specificity, samples from cancer and cancer-free patients must be tested and compared with other clinically approved methods. For this, each sample needs to be serially diluted until the HE4 concentration falls within the working region of this assay. The past dataset on variations of HE4 concentrations of healthy and cancerous samples can be helpful to approximately determine the extent of dilution. Diluted samples of the

unknown sample can be used for conjugation with antibody-modified magnetic beads. Then, following the similar steps explained in the experimental section, the final conjugate can be purified and tested with LIBS for the Si intensity measurements. Finally, by interpolating the Si intensity of the conjugate on the working region of the assay, one can determine the unknown concentration of HE4. To confirm the concentration of the unknown sample, the sample can be further diluted or concentrated within the working region of this assay and can be tested similarly.

However, this method has a few challenges before being implemented in clinical trials. Since our working region is 0.0–0.0073 pM, a serial dilution process would be required to utilize this method. Potential errors associated with dilution might cause overdiagnoses. Since the working region of this assay is narrow, a higher number of dilution steps is required so that the serum concentration can fall within the working region of this assay. The number of dilution steps can be reduced by higher volumes of buffer solution to small amounts of the sample so that the error associated with every single step can be minimized. Second, non-selective cross-coupling can challenge the reliability of this assay. The complex nature of biomolecules containing many nucleophilic functional groups, such as amines, thiols, hydroxyl groups, and carboxylates, makes bioconjugation a challenge. These other biomolecules could yield other non-specific byproducts, challenging the purification, detection, and quantification process.[50] As explained before, the silicon signal observed in the control experiment mainly arises from these non-specific conjugations. We eliminated this cross-coupling effect by doing control experiments (conjugation of the antibody without HE4, conjugation without both HE4 and antibody, and measuring the signal of the magnetic beads only) so that it did not affect getting a linear regression between silicon intensity with the HE4 concentration. However, the amount of cross-coupling could still differ with the HE4 concentration. The available binding sites for the cross-coupling might be altered depending on the amount of HE4 in the conjugation medium. Additionally, the HE4 could also block the silica particles from being directly bound with the magnetic beads, and this effect could vary depending on the amount of HE4 present in the medium. Due to these reasons, one cannot expect consistency in cross-coupling, as seen in this assay. Blocking agents can disable the potential active sites of the antibody or protein A to prevent the silica from making non-specific conjugations with antibodies or magnetic beads to help tackle the cross-coupling issues. This requires careful structural and chemical reaction knowledge of biomolecules. Alternatively, a size filtration process could also be followed to separate the HE4-modified beads from bare magnetic beads or magnetic beads with the antibody responsible for cross-coupling.

## CONCLUSIONS

In this work, sandwiching an antibody–antigen complex using two different types of microparticles through bioconjugation was attempted to detect and quantify the ovarian cancer antigen HE4 at significantly low concentrations. Once the expected conjugation was achieved, purification and detection were the key steps; for this purpose, we used iron and silica microparticles, respectively. Using a magnetic separator, the final conjugate was purified from the buffer solution before detecting the silicon emission using LIBS. A linear working region was achieved regarding silicon intensity and the HE4
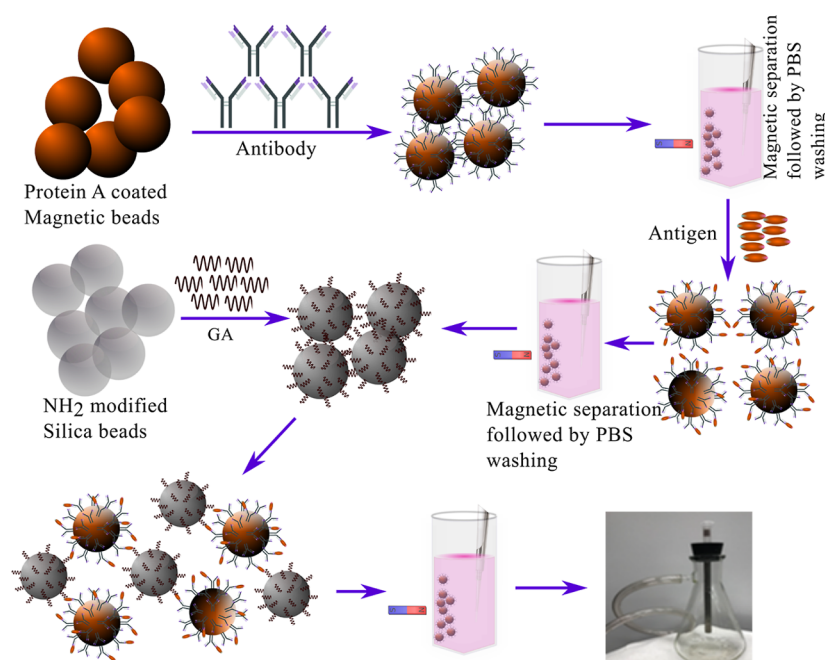
**Figure 8.** Schematic diagram of the magnetic particle-based immunoassay system for the isolation and purification of HE4 protein biomarkers.

concentration to find the unknown HE4 concentration. The developed assay was detected below 0.0073 pM, with the lowest detection limit of 0.0022 pM. In addition, we estimated the amount of bound silica particles with the HE4 antigen and deduced the coupling ratio of silica particles to antigens, which was calculated through two different analyses, peak height and area. For this goal, a silicon calibration curve was utilized. Moreover, not only were the silica particles bound with HE4 established but we calculated the cross-coupled particles with magnetic beads. Finally, we discussed the issues associated with this assay when implementing it in clinical trials and potential solutions to minimize those issues.

## MATERIALS AND METHODOLOGY

A sandwich-type immunoassay method uses iron and silica microparticles to sandwich the antibody−antigen conjugate through bioconjugation. The conjugation steps in this study are depicted in Figure 8 and are briefly described in the following. Protein A-modified iron particles are coupled to anti-HE4 antibodies, which are then incubated with the antigen such that the antibody can bind to the antigen. Later, this conjugate is mixed with GA-modified silica microparticles to develop a sandwich-type immunoassay. A magnetic separation method was followed to purify the silica particles that were conjugated to the antibody−antigen complex, and then we used LIBS to detect the silica particles to quantify the extracted HE4 antigen.

**Preparation of Silica Particle Suspension for Calibration.** First, 1 mg of silica particles (1 $\mu$m in diameter, purchased from Bangs Laboratories) were mixed with 1 mL of phosphate buffer saline (PBS-pH 7.4) to create a silica stock suspension. Nine sample sets of silica microparticle suspensions were prepared from this stock suspension. A series of different amounts of silica particles having 0 $\mu$g (control), 0.01, 0.1, 0.5, 1, 2, 5, 10, and 100 $\mu$g weight loads in PBS suspension were prepared.

Then, each of the concentrations was mixed with a standard amount of 50 $\mu$g of ~1.5 $\mu$m iron microparticles (magnetic

beads). These particles were filtered through a centrifugal filter with a 0.45 $\mu$m pore size in a polyethersulfone membrane filter (Sartorius Stedim Biotech) and allowed to dry for over 1 h at ambient temperature. To achieve homogeneous sample distribution on the filter surface, the particle suspension was vortexed, and then the buffer was removed by applying negative partial pressure to the bottom part of the filter. These sets were used with the LIBS setup to create a calibration curve to compare our sandwich assay results for quantification purposes.

**Antibody−Protein A-Coated Magnetic Bead Conjugation.** A 2.2 mg/mL stockpile of anti-HE4 monoclonal antibodies (HM170 from the Biotechnology company East Coast Bio, Inc) was used. Then, the suspension was diluted using a serial dilution process to yield a pre-determined number of antibodies per sample (~5.28 × 10$^6$ antibodies/sample). Protein A-coated magnetic beads (10 $\mu$L, density 5 mg/mL) from Bangs Laboratories were first washed with PBS to remove unbound protein A. Then, the magnetic beads were mixed with antibodies using a Fisherbrand Mini Tube Rotator (Fisher Scientific) at the rate of 40 rpm for 3 h for conjugation. The antibody-conjugated particles were magnetically separated, and the supernatant (post-coupling solution) was discarded. Antibody-coated particles were further washed three times with PBS to remove nonspecifically bound antibodies, followed by magnetic separation and discarding of the wash supernatant.

**Conjugation of the Antigen and the Antibody.** Predetermined concentrations of HE4 antigens (0.0018, 0.0073, 0.0146, 0.0292, and 0.4671 pM) were prepared by diluting 10 $\mu$L of antigen stock suspension (East Coast Bio, LA306, 500 pmol/mL) using PBS. After that, those concentrations were mixed with the magnetic bead/antibody complex and incubated overnight. To each of the five samples, various amounts of PBS (pH 7.4) were added such that the final volume of all five samples equaled 150 $\mu$L. After overnight incubation, antigen-conjugated beads were magnetically

separated and washed three times with PBS to remove the nonspecifically bound antigens.

**Conjugation of Silica Particles with Antigen-Coated Magnetic Beads.** A 1 mg quantity of amine-modified silica particles (Bangs Laboratories) was mixed with 50 $\mu$L of 25% GA and allowed to mix on a rotator overnight at the rate of 40 rpm. After that, 950 $\mu$L of PBS was added to make the final volume 1000 $\mu$L. The antigen-conjugated particles were incubated with 10 $\mu$L (=10 $\mu$g of suspended particles) of the GA-modified silica particle suspension and left on a rotator for 3 h so that the silica particles could bind to the antigen through the GA. Then, conjugated particles were magnetically separated and washed three times with PBS to remove unbound constituents. Finally, 150 $\mu$L of PBS was added to this conjugate to make a suspension and then filtered through the centrifugal filter (pore size of 0.45 $\mu$m) by applying negative pressure so that the conjugate would be uniformly spread over the filter for LIBS measurements.

## ■ ASSOCIATED CONTENT

### ⓢ Supporting Information

The Supporting Information is available free of charge at https://pubs.acs.org/doi/10.1021/acs.bioconjchem.2c00551.

Full range graphs for Si I, Fe I, Fe II, and C I emissions; complete Fisher's family-wise mean comparison test results; and evaluation of selectivity and specificity (PDF)

## ■ AUTHOR INFORMATION

### Corresponding Author

**Poopalasingam Sivakumar** − *School of Physics and Applied Physics, Southern Illinois University Carbondale, Carbondale, Illinois 62901, United States;* ⓞ orcid.org/0000-0001-5250-9325; Phone: +1-618-453-2272; Email: psivakumar@siu.edu

### Authors

**Robinson Karunanithy** − *School of Physics and Applied Physics, Southern Illinois University Carbondale, Carbondale, Illinois 62901, United States*

**Suthakaran Ratnasingam** − *Department of Mathematics, California State University, San Bernardino, California 92407, United States*

**Torrey Holland** − *School of Physics and Applied Physics, Southern Illinois University Carbondale, Carbondale, Illinois 62901, United States; Department of Life and Physical Science, John A. Logan College, Carterville, Illinois 62918, United States*

Complete contact information is available at:
https://pubs.acs.org/10.1021/acs.bioconjchem.2c00551

### Notes

The authors declare no competing financial interest.

## ■ REFERENCES

(1) American Cancer Society. https://www.cancer.org/cancer/ovarian-cancer/about/key-statistics.html (accessed Oct 02, 2022).

(2) Siegel, R. L.; Miller, K. D.; Jemal, A. Cancer statistics, 2019. *Ca-Cancer J. Clin.* **2019**, *69*, 7−34.

(3) Hazelton, W. D.; Luebeck, E. G. Biomarker-Based Early Cancer Detection: Is It Achievable? *Sci. Transl. Med.* **2011**, *3*, 109fs9.

(4) Das, P. M.; Bast Jr, R. C., Jr Early Detection of Ovarian Cancer. *Biomarkers Med.* **2008**, *2*, 291−303.

(5) Visintin, I.; Feng, Z.; Longton, G.; Ward, D. C.; Alvero, A. B.; Lai, Y.; Tenthorey, J.; Leiser, A.; Flores-Saaib, R.; Yu, H.; et al. Diagnostic Markers for Early Detection of Ovarian Cancer. *Clin. Cancer Res.* **2008**, *14*, 1065−1072.

(6) Abramowicz, J. S.; Timmerman, D. Ovarian Mass−Differentiating Benign from Malignant: The Value of the International Ovarian Tumor Analysis Ultrasound Rules. *Am. J. Obstet. Gynecol.* **2017**, *217*, 652−660.

(7) Sarojini, S.; Tamir, A.; Lim, H.; Li, S.; Zhang, S.; Goy, A.; Pecora, A.; Suh, K. S. Early Detection Biomarkers for Ovarian Cancer. *J. Oncol.* **2012**, *2012*, 1−15.

(8) Moss, E. L. The Role of CA125 in Clinical Practice. *J. Clin. Pathol.* **2005**, *58*, 308−312.

(9) Niloff, J. M.; Klug, T. L.; Schaetzl, E.; Zurawski, V. R., Jr.; Knapp, R. C.; Bast, R. C., Jr. Elevation of Serum CA125 in Carcinomas of the Fallopian Tube, Endometrium, and Endocervix. *Am. J. Obstet. Gynecol.* **1984**, *148*, 1057−1059.

(10) Barbieri, R. L.; Niloff, J. M.; Bast, R. C., Jr.; Schaetzl, E.; Kistner, R. W.; Knapp, R. C. Elevated Serum Concentrations of CA-125 in Patients with Advanced Endometriosis. *Fertil. Steril.* **1986**, *45*, 630−634.

(11) Kafali, H.; Artuc, H.; Demir, N. Use of CA125 Fluctuation during the Menstrual Cycle as a Tool in the Clinical Diagnosis of Endometriosis; a Preliminary Report. *Eur. J. Obstet. Gynecol. Reprod. Biol.* **2004**, *116*, 85−88.

(12) Niloff, J. M.; Knapp, R. C.; Schaetzl, E.; Reynolds, C.; Bast, R. C., Jr CA125 Antigen Levels in Obstetric and Gynecologic Patients. *Obstet. Gynecol.* **1984**, *64*, 703.

(13) Atallah, G. A.; Abd. Aziz, N. H.; Teik, C. K.; Shafiee, M. N.; Kampan, N. C. New Predictive Biomarkers for Ovarian Cancer. *Diagnostics* **2021**, *11*, 465.

(14) Charkhchi, P.; Cybulski, C.; Gronwald, J.; Wong, F. O.; Narod, S. A.; Akbari, M. R. CA125 and Ovarian Cancer: A Comprehensive Review. *Cancers* **2020**, *12*, 3730.

(15) Dochez, V.; Caillon, H.; Vaucel, E.; Dimet, J.; Winer, N.; Ducarme, G. Biomarkers and Algorithms for Diagnosis of Ovarian Cancer: CA125, HE4, RMI and ROMA, a Review. *J. Ovarian Res.* **2019**, *12*, 28.

(16) Havrilesky, L. J.; Whitehead, C. M.; Rubatt, J. M.; Cheek, R. L.; Groelke, J.; He, Q.; Malinowski, D. P.; Fischer, T. J.; Berchuck, A. Evaluation of Biomarker Panels for Early Stage Ovarian Cancer Detection and Monitoring for Disease Recurrence. *Gynecol. Oncol.* **2008**, *110*, 374−382.

(17) Moore, R. G.; Brown, A. K.; Miller, M. C.; Skates, S.; Allard, W. J.; Verch, T.; Steinhoff, M.; Messerlian, G.; DiSilvestro, P.; Granai, C. O.; et al. The Use of Multiple Novel Tumor Biomarkers for the Detection of Ovarian Carcinoma in Patients with a Pelvic Mass. *Gynecol. Oncol.* **2008**, *108*, 402−408.

(18) Yamashita, M.; Fenn, J. B. Electrospray Ion Source. Another Variation on the Free-Jet Theme. *J. Phys. Chem.* **1984**, *88*, 4451−4459.

(19) Wolters, D. A.; Washburn, M. P.; Yates, J. R. An Automated Multidimensional Protein Identification Technology for Shotgun Proteomics. *Anal. Chem.* **2001**, *73*, 5683−5690.

(20) Chen, S.; Qamar, A. Z.; Asefifeyzabadi, N.; Funneman, M.; Taki, M.; Elliot, L.; Kinsel, M. E.; Kinsel, G. R.; Shamsi, M. H. Hand-Fabricated CNT/AgNPs Electrodes Using Wax-on-Plastic Platforms for Electro-Immunosensing Application. *Sci. Rep.* **2019**, *9*, 6131.

(21) Burnette, W. N. "Western Blotting": Electrophoretic Transfer of Proteins from Sodium Dodecyl Sulfate-Polyacrylamide Gels to Unmodified Nitrocellulose and Radiographic Detection with Antibody and Radioiodinated Protein A. *Anal. Biochem.* **1981**, *112*, 195−203.

(22) Li, J.; Li, X.; Huang, Y.; Zhong, Y.; Lan, Q.; Wu, X.; Hu, R.; Zhang, G.; Hu, X.; Yang, Z. Biofunctionalized Mesoporous Silica Nanospheres for the Ultrasensitive Chemiluminescence Immunoassay of Tumor Markers. *New J. Chem.* **2018**, *42*, 11264−11267.

(23) Cao, J.; Ouyang, P.; Yu, S.; Shi, F.; Ren, C.; Wang, C.; Shen, M.; Yang, Z. Hedgehog-like Bi $_2$ S $_3$ Nanostructures: A Novel Composite Soft Template Route to the Synthesis and Sensitive Electrochemical Immunoassay of the Liver Cancer Biomarker. *Chem. Commun.* **2021**, *57*, 1766−1769.

(24) Mennink-Kersten, M. A.; Donnelly, J. P.; Verweij, P. E. Detection of Circulating Galactomannan for the Diagnosis and Management of Invasive Aspergillosis. *Lancet Infect. Dis.* **2004**, *4*, 349−357.

(25) Nielsen, U. B.; Cardone, M. H.; Sinskey, A. J.; MacBeath, G.; Sorger, P. K. Profiling Receptor Tyrosine Kinase Activation by Using Ab Microarrays. *Proc. Natl. Acad. Sci.* **2003**, *100*, 9330−9335.

(26) Yang, Z.; Lan, Q.; Li, J.; Wu, J.; Tang, Y.; Hu, X. Efficient Streptavidin-Functionalized Nitrogen-Doped Graphene for the Development of Highly Sensitive Electrochemical Immunosensor. *Biosens. Bioelectron.* **2017**, *89*, 312−318.

(27) Markushin, Y.; Sivakumar, P.; Connolly, D.; Melikechi, N. Tag-Femtosecond Laser-Induced Breakdown Spectroscopy for the Sensitive Detection of Cancer Antigen 125 in Blood Plasma. *Anal. Bioanal. Chem.* **2015**, *407*, 1849−1855.

(28) Markushin, Y.; Melikechi, N.; Marcano O, O. A.; Rock, S.; Henderson, E.; Connolly, D. LIBS-Based Multi-Element Coded Assay for Ovarian Cancer Application. *Proceedings of SPIE-The International Society for Optical Engineering 7190*; Achilefu, S., Raghavachari, R., Eds.: San Jose, CA, 2009; p 719015..

(29) Melikechi, N.; Markushin, Y. Mono- and Multi-Element Coded Libs Assays and Methods. U.S. Patent 20110171636 A1, 2011.

(30) Robinson, K. *Micro-Particles Immunoassays for Early Detection of Ovarian Cancer Using Laser Induced Breakdown Spectroscopy*; University of illinois Urbana Champaign, 2021. https://ui.adsabs.harvard.edu/link_gateway/2021isms.confERF01K/doi:10.15278/isms.2021.RF01.

(31) Karunanithy, R.; Holland, T.; Sivakumar, P. Influence of Glutaraldehyde's Molecular Transformations on Spectroscopic Investigations of Its Conjugation with Amine-Modified Fe $_3$ O $_4$ Microparticles in the Reaction Medium. *Langmuir* **2021**, *37*, 5242−5251.

(32) Yang, R.; Bi, L. Spectral Enhancement Mechanism and Analysis of Defocused Collinear DP-LIBS Technology. *Optik* **2021**, *243*, 167025.

(33) Li, C.; Feng, C.-L.; Oderji, H. Y.; Luo, G.-N.; Ding, H.-B. Review of LIBS Application in Nuclear Fusion Technology. *Front. Physiol.* **2016**, *11*, 114214.

(34) Bhatt, C. R.; Ghany, C. T.; Yueh, F. Y.; Singh, J. P.; McIntyre, D. L. Laser-Induced Breakdown Spectroscopy. In *Molecular and Laser Spectroscopy*; Elsevier, 2018; pp 265−282.

(35) Pamu, R.; Davari, S. A.; Darbar, D.; Self, E. C.; Nanda, J.; Mukherjee, D. Calibration-Free Quantitative Analysis of Lithium-Ion Battery (LiB) Electrode Materials Using Laser-Induced Breakdown Spectroscopy (LIBS). *ACS Appl. Energy Mater.* **2021**, *4*, 7259−7267.

(36) Andrade, D. F.; Pereira-Filho, E. R. Direct Determination of Contaminants and Major and Minor Nutrients in Solid Fertilizers Using Laser-Induced Breakdown Spectroscopy (LIBS). *J. Agric. Food Chem.* **2016**, *64*, 7890−7898.

(37) Moros, J.; ElFaham, M. M.; Laserna, J. J. Dual-Spectroscopy Platform for the Surveillance of Mars Mineralogy Using a Decisions Fusion Architecture on Simultaneous LIBS-Raman Data. *Anal. Chem.* **2018**, *90*, 2079−2087.

(38) Multari, R. A.; Cremers, D. A.; Scott, T.; Kendrick, P. Detection of Pesticides and Dioxins in Tissue Fats and Rendering Oils Using Laser-Induced Breakdown Spectroscopy (LIBS). *J. Agric. Food Chem.* **2013**, *61*, 2348−2357.

(39) Harmon, R. S.; Senesi, G. S. Laser-Induced Breakdown Spectroscopy − A Geochemical Tool for the 21st Century. *Appl. Geochem.* **2021**, *128*, 104929.

(40) Yao, S.; Yao, X.; Zhang, L.; Qin, H.; Yu, Z.; Chen, X.; Lu, Z.; Lu, J. Improving the LIBS Quantitative Analysis of Unburned Carbon in Fly Ash Based on the Optimization of Reference Value. *Energy Fuels* **2020**, *34*, 6483−6489.

(41) Cheng, X.; Yang, X.; Zhu, Z.; Guo, L.; Li, X.; Lu, Y.; Zeng, X. On-Stream Analysis of Iron Ore Slurry Using Laser-Induced Breakdown Spectroscopy. *Appl. Opt.* **2017**, *56*, 9144.

(42) NIST. https://physics.nist.gov/PhysRefData/ASD/LIBS/libs-form.html (accessed Oct 23, 2021).

(43) Ramezanian, Z.; Darbani, S. M. R.; Majd, A. E. Effect of Self-Absorption Correction on Surface Hardness Estimation of Fe−Cr−Ni Alloys via LIBS. *Appl. Opt.* **2017**, *56*, 6917.

(44) Yuan, T.; Wang, Z.; Li, L.; Hou, Z.; Li, Z.; Ni, W. Quantitative Carbon Measurement in Anthracite Using Laser-Induced Breakdown Spectroscopy with Binder. *Appl. Opt.* **2012**, *51*, B22.

(45) Huang, J.-S.; Ke, C.-B.; Lin, K.-C. Matrix Effect on Emission/Current Correlated Analysis in Laser-Induced Breakdown Spectroscopy of Liquid Droplets. *Spectrochim. Acta, Part B* **2004**, *59*, 321−326.

(46) Yue, Z.; Sun, C.; Gao, L.; Zhang, Y.; Shabbir, S.; Xu, W.; Wu, M.; Zou, L.; Tan, Y.; Chen, F.; et al. Machine Learning Efficiently Corrects LIBS Spectrum Variation Due to Change of Laser Fluence. *Opt. Express* **2020**, *28*, 14345.

(47) Hahn, D. W.; Omenetto, N. Laser-Induced Breakdown Spectroscopy (LIBS), Part II: Review of Instrumental and Methodological Approaches to Material Analysis and Applications to Different Fields. *Appl. Spectrosc.* **2012**, *66*, 347−419.

(48) Wang, Z.; Li, L.; West, L.; Li, Z.; Ni, W. A Spectrum Standardization Approach for Laser-Induced Breakdown Spectroscopy Measurements. *Spectrochim. Acta, Part B* **2012**, *68*, 58−64.

(49) Zaytsev, S. M.; Krylov, I. N.; Popov, A. M.; Zorov, N. B.; Labutin, T. A. Accuracy Enhancement of a Multivariate Calibration for Lead Determination in Soils by Laser Induced Breakdown Spectroscopy. *Spectrochim. Acta, Part B* **2018**, *140*, 65−72.

(50) Zhang, C.; Vinogradova, E. V.; Spokoyny, A. M.; Buchwald, S. L.; Pentelute, B. L. Arylation Chemistry for Bioconjugation. *Angew. Chem., Int. Ed.* **2019**, *58*, 4810−4839.